Numerical simulation of water flow in an axial flow pump with adjustable guide vanes [†]

Zhongdong QIAN[1], Yan WANG[1], Wenxin HUAI[1] and Youngho LEE[2,*]

[1]*State Key Laboratory of Water Resources and Hydropower Engineering Science, Wuhan University, Wuhan 430072, P. R. China*
[2]*Division of Mechanical and Information Engineering, Korea Maritime University, Busan 606-791, Korea*

Abstract

A new adjustable guide vane (AGV) is proposed in this paper. This vane can reduce hydraulic losses and improve the performance of an axial flow pump. The formula of AGV adjustment was obtained after theoretical analysis. The fluid flow inside the axial flow pump with a fixed guide vane and adjustable guide vane was simulated. The calculated Q-H curves for the fixed guide vane agreed well with the experimental ones. The results show that the attack angle and flow separation have an important contribution to the vortices which create hydraulic losses in the guide vane channel. The AGV can decrease hydraulic losses and significantly enhance the pump head and efficiency by changing the guide vane angle.

Keywords: Adjustable guide vanes; Axial flow pump; Hydraulic performance; Numerical simulation

---

1. Introduction

With the increasing application of an axial flow pump, the improvement of its efficiency continues to become more and more important. One of the most useful methods to increase its efficiency is the installation of a guide vane behind the pump impeller [1]. Guide vanes can improve the head and efficiency of the pump by transforming the kinetic energy of the rotating flow, which has a tangential velocity component, into pressure energy. When the pump is working under off-design condition, the attack angle, which causes hydraulic loss, will always exist at the leading edge of the guide vane. This is because the traditional guide vane is fixed on the guide vane hub with a fixed angle for the design condition and cannot be adjusted with the change in working conditions. Studies have shown that the fixed guide vane can generally retrieve about 10% of the kinetic energy [2]. This paper proposes a new adjustable guide vane which can reduce hydraulic loss and improve the performance of the axial flow pump through adjustment of the guide vane angle under off-design conditions.

The internal flow field of the axial flow pump is difficult to measure due to rotor-stator interaction. Thus, Computational Fluid Dynamics (CFD) has been an effective tool in studies on the internal flow field in pumps and turbines [3-7]. In this paper, the three-dimensional steady turbulent flow inside the full passage of a model axial flow pump was simulated using CFD. A comparison of the computational head and experimental head was conducted to verify the mathematical model. The influence of AGV on the head, efficiency, and energy character was analyzed, and the theorem for adjusting the AGV angle was given.

2. Physical model

The model axial flow pump impeller for this computation is ZM60. The computational domain is the flow passage from the inlet to the outlet, including the impeller and guide vanes as shown in Fig. 1. There were four impeller blades. The diameter of the impeller was 0.3m, the hub ratio 0.5133, the rated speed was 1450r/min, and the number of guide vane blades was five. All these structures are shown in Fig. 2.

The structured mesh was used for the inlet and outlet, while the unstructured mesh was used for the impeller and guide vanes due to their complicated geometry. The total number of cells is about one million. The mesh of the model is shown in Fig. 3.

3. Mathematical model

The three-dimensional Reynolds-averaged Navier-Stokes equations for uncompressible flow are as follows [8]:
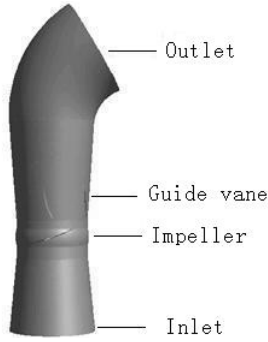

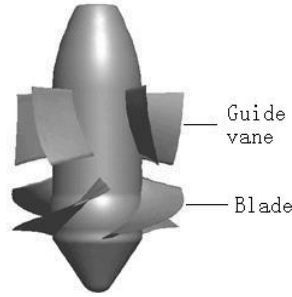Fig. 1. The whole flow passage axial flow pump model.
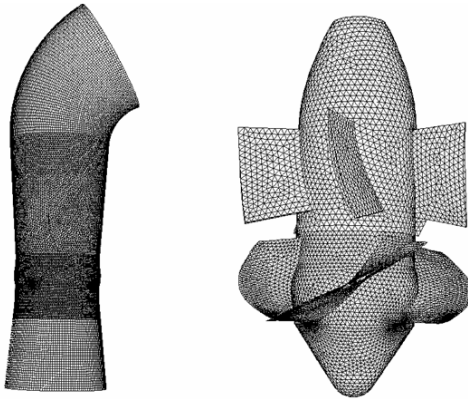

Fig. 2. The impeller and guide vane.

Fig. 3. The mesh of the model.

$$\frac{\partial \rho}{\partial t} + \frac{\partial}{\partial x_i}(\rho u_i) = 0 \tag{1}$$

$$\frac{\partial(\rho u_i)}{\partial t} + \frac{\partial(\rho u_i u_j)}{\partial x_j} = -\frac{\partial p}{\partial x_i} + \frac{\partial}{\partial x_j}\left(\mu \frac{\partial u_i}{\partial x_j}\right) + \frac{\partial \tau_{ij}}{\partial x_j} \tag{2}$$

where $\tau_{ij} = -\rho \overline{u_i' u_j'}$ is the Reynolds stress.

The $k - \varepsilon$ model was chosen to enclose the equations. Considering the rotating flow inside the pump impeller, the RNG $k - \varepsilon$ model, which is adaptive for strongly rotating flow, was used in this simulation [9, 10].

$$\frac{\partial(\rho k)}{\partial t} + \frac{\partial(\rho k u_i)}{\partial x_i} = \frac{\partial}{\partial x_j}\left[\left(\mu + \frac{\mu_t}{\sigma_k}\right)\frac{\partial k}{\partial x_j}\right] + G_k + \rho \varepsilon \tag{3}$$

$$\frac{\partial(\rho \varepsilon)}{\partial t} + \frac{\partial(\rho \varepsilon u_i)}{\partial x_i} = \frac{\partial}{\partial x_j}\left[\left(\mu + \frac{\mu_t}{\sigma_\varepsilon}\right)\frac{\partial k}{\partial x_j}\right] + \frac{C_{1\varepsilon}^* \varepsilon}{k} G_k - C_{2\varepsilon}\rho \frac{\varepsilon^2}{k} \tag{4}$$
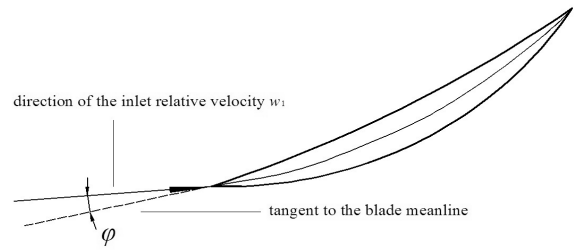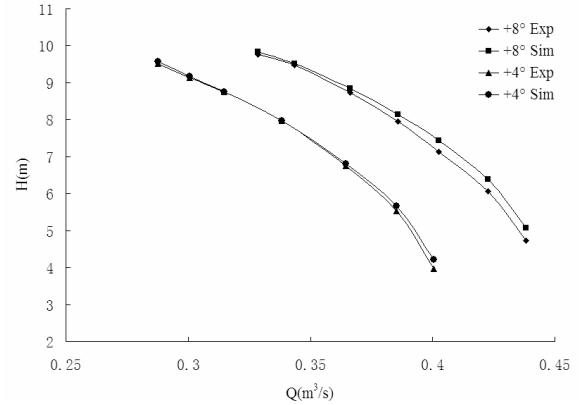

Fig. 4. Schematic diagram of the blade setting angle.

Fig. 5. Comparison of the Q-H curve.

where the model constants were chosen from Ref. 10. For the RNG $k - \varepsilon$ model, the Reynolds stress can be written as

$$\tau_{ij} = \mu_t\left(\frac{\partial u_i}{\partial x_j} + \frac{\partial u_j}{\partial x_i}\right) - \frac{2}{3}\left(\rho k + \mu_t \frac{\partial u_i}{\partial x_i}\right)\delta_{ij} \tag{5}$$

Meanwhile, the turbulent kinetic viscosity coefficient can be written as

$$\mu_t = \rho C_\mu \frac{k^2}{\varepsilon} \tag{6}$$

All simulations were conducted using the commercial CFD software Fluent 6.3. The SIMPLEC algorithm was used for the pressure-velocity coupling [11, 12]. The second order upwind difference scheme was used for the momentum, turbulent kinetic energy, and dissipation rate equations. The mass flow rate was defined for the inlet and the static pressure for the outlet. The roughness height of the hub and casing was also considered [13]. The sliding mesh model was used to simulate the rotor-stator interaction in the pump. In the sliding mesh technique provided by Fluent 6.3, the interface zones of adjacent cell zones were associated with one another to form a "grid interface." The two cell zones move relative to each other along the grid interface.

4. Results and discussions

Seven operating points for the +4° and +8° of the blade-setting angle with the fixed-guide vanes were computed to
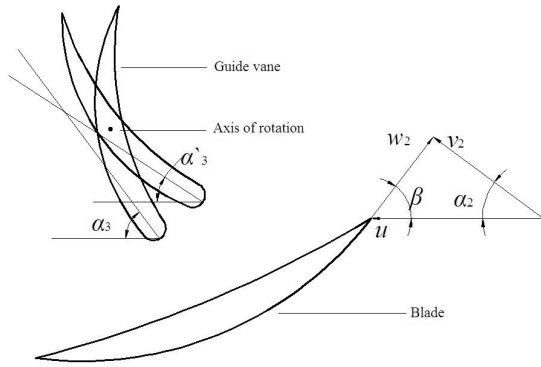
Fig. 6. Schematic diagram of AGV adjustment.

Table 1. Computational points and the corresponding angle for the +4° blade setting angle.

Q (m³/s)	0.28779	0.30078	0.31483	0.33837	0.36469	0.38518	0.40046
α_3' (°)	39.065	40.734	45.503	45.377	48.451	50.737	52.380
$\Delta\alpha$ (°)	9.435	7.766	5.997	3.123	0.049	-2.237	-3.880

Table 2. Computational points and the corresponding angle for the +8° blade setting angle.

Q (m³/s)	0.3285	0.34364	0.36612	0.38577	0.40252	0.4226	0.43826
α_3' (°)	42.321	44.018	46.452	48.494	50.172	52.107	53.559
$\Delta\alpha$ (°)	6.179	4.482	2.048	0.006	-1.672	-3.607	-5.059

Fig. 7. Comparison of the Q-H curves.

Fig. 8. Comparison of the Q-η curves.

validate the mathematical model. Fig. 4 shows the blade-setting angle, which is determined by angle φ between the tangent to the blade meanline and the direction of the inlet relative velocity w_1 at the front-edge point of the blade. Angle $\varphi = 0$ was assumed as the impeller design angle.

The computational results of the flow discharge (Q)-head (H) curves and the experimental ones are shown in Fig. 5.

Fig. 5 shows that the computational results agree well with the experimental ones, with a maximum error of less than 5%. The difference comes from the tip clearance flow which was not considered in this computation at large discharge condition [14].

The design of guide vanes is usually aimed at improving flow pattern and reducing hydraulic loss by converting some of the kinetic energy into pressure energy. Therefore, the inlet flow angle of the vane should be consistent with the outlet flow angle of the impeller blade at design condition. However, the consistency cannot be maintained at off-design conditions because of the variation of the outlet flow angle of the impeller. The angle of attack of the guide vane is not zero, and the hydraulic loss increases.

Adjustable guide vanes (AGV) are intended to change the vane angle to maintain the shock free flow pattern. The schematic diagram of AGV is shown in Fig. 6. The basic idea of the AGV is that the guide vane inlet flow angle α_3 should be adjusted according to the impeller outlet flowing angle α_2 to reduce shock loss. α_2 can be derived from the velocity triangle when the blade angle and discharge are known.

As shown in Fig. 6, u is the circular velocity, v_2 is the outlet absolute velocity, w_2 is the outlet relative velocity, α_2 is the outlet absolute flow angle, β is the outlet relative flow angle, α_3 is the design fixed guide vane inlet flow angle, and α_3' is the rational guide vane inlet flow angle. The computational section is a cylindrical section at the tip of the blade whose radius is equal to 0.15m. The formula of α_2 can be derived from the velocity triangle and discharge as follows:

$$\alpha_2 = \arctan\left(\frac{60Q}{2\pi^2\left(R^2 - r^2\right)Rn - 60Q\cot\beta}\right) \quad (7)$$
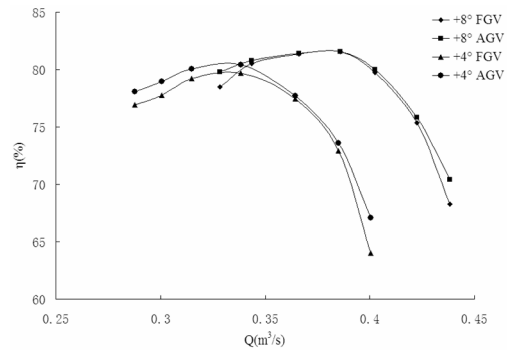
where Q is the discharge, R is the radius of the pump shell

at the impeller outlet, r is the hub radius, and n is the impeller speed.

According to the principle of guide vane design, the formula of the rational guide vane inlet flow angle α_3' can be written as follows [15]:

$$\alpha_3' = \arctan\left(\frac{\tan\alpha_2}{\psi_3}\right) \quad (8)$$

where $\psi_3 = 1 - \dfrac{zs_{u3}}{D_3\pi}$; Z is the blade number of the guide vane; D_3 is the diameter of the computational section; and s_{u3} is the circumferential directional thickness of the guide vane inlet.

The angle deviation is $\Delta\alpha = \alpha_3 - \alpha_3'$. In this computation, the design α_3 is known as $\alpha_3 = 48.5^0$. The angle deviation
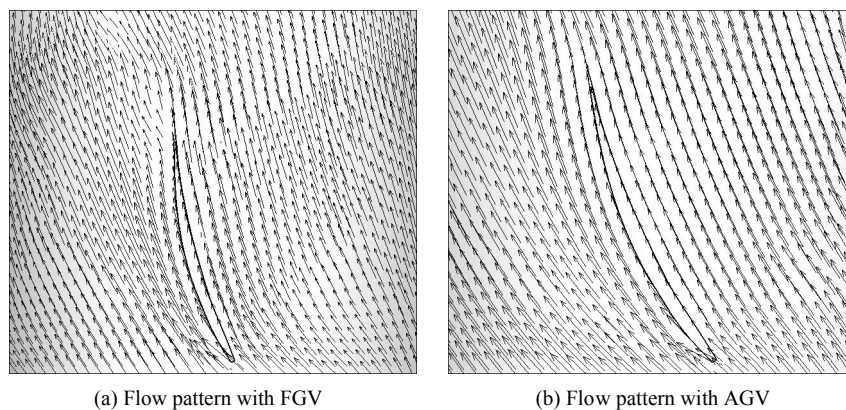
| (a) Flow pattern with FGV | (b) Flow pattern with AGV |

Fig. 9. Flow pattern at the minimum flow condition of +4° blade setting angle.

| (a) Flow pattern before adjustment | (b) Flow pattern after adjustment |

Fig. 10. Flow pattern at the maximum flow condition of +4° blade setting angle.

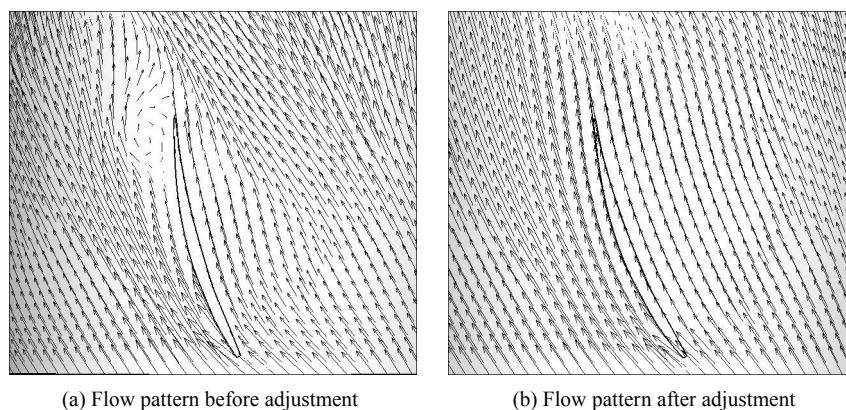| (a) Flow pattern before adjustment | (b) Flow pattern after adjustment |
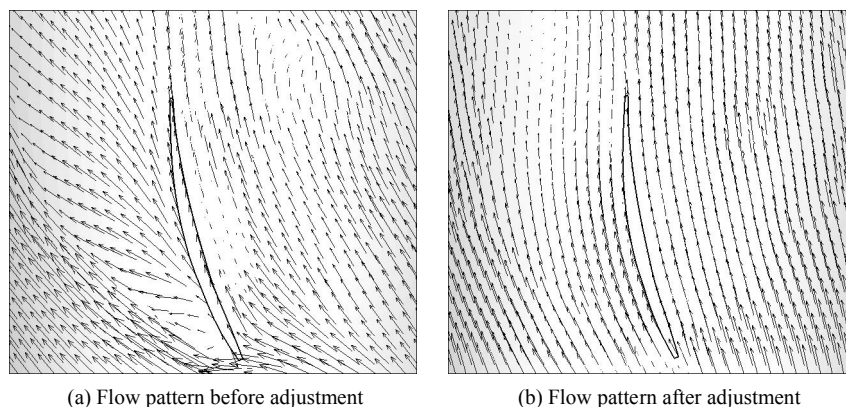
Fig. 11. Flow pattern at the minimum flow condition of +8° blade setting angle.

$\Delta \alpha$ for each operating point is shown in Tables 1 and 2.

Based on the full passage computation of the axial flow pump with fixed guide vanes (FGV) and AGV, the Q-H curves and Q-η (efficiency) curves are shown in Figs. 7 and 8.

The results show that the AGV was more efficient in improving the performance of the axial flow pump than the FGV at off-design condition. For the +4° blade setting angle, the head increased by 0.213 m, while the efficiency increased by 1.178% at the minimum discharge condition. At the maximum discharge condition, it increased by 0.437 m and 3.089%,

respectively. For the +8° blade setting angle, the head increased by 0.167 m, while the efficiency increased by 1.29% at the minimum discharge condition and 0.496 m and 2.165%, respectively, at the maximum discharge condition.

The flow patterns in the guide vane channel at minimum and maximum discharge conditions are shown in Figs. 9 to 12. These figures show that the vortices appeared at the tailing edge of the fixed guide vane at low discharge condition, while the flow separation appeared at the leading edge at large discharge condition. The vortex and flow separation are known

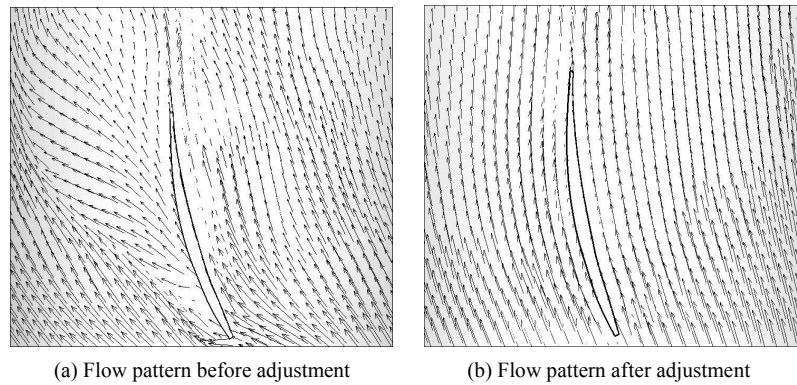| (a) Flow pattern before adjustment | (b) Flow pattern after adjustment |

Fig. 12. Flow pattern at the maximum flow condition of +8° blade setting angle.

as the main contributors of hydraulic losses. The vortex and flow separation were caused by different attack angles at different discharges. With the application of AGV, the attack angle of the guide vane is almost zero. The vortex and flow separation caused by the attack angle disappeared, and flow pattern improved accordingly. As a result, the hydraulic losses caused by the vortex and flow separation were decreased, and the head and efficiency of the axial flow pump was enhanced.

5. Conclusion

Simulations of the three-dimensional steady flow in an axial flow pump with FGV and AGV were conducted using the commercial CFD software Fluent 6.3. The results show the following:

(I) The mathematical model used in this paper can accurately simulate the flow field inside the axial flow pump. The computational Q-H curves agree well with the experimental ones.

(II) The theorem of AGV adjustment was deduced from the impeller outlet velocity triangle and the principle of guide vane design.

(III) The AGV can reduce the negative influences of attack angle and improve the flow pattern in the guide vane channel effectively, significantly decreasing hydraulic loss.

(IV) The AGV can significantly improve the head and efficiency of the pump at off-design conditions. In this simulation, the maximum improvement of the head and the efficiency were 0.496 m and 3.089%, respectively.

Acknowledgements

Nomenclature——————————————————

D	:	Diameter [m]
H	:	Head [m]
n	:	Revolution per minute [rpm]
Q	:	Flow rate [m³/s]

R	:	Radius of the pump shell at the impeller outlet [m]
r	:	Hub radius [m]
S	:	Circumferential directional thickness of the guide vane inlet [m]
t	:	Time [s]
u	:	Circular velocity [m/s]
v	:	Absolute velocity [m/s]
w	:	Relative velocity [m/s]
Z	:	Blade number of the guide vane
α	:	Flow angle [deg]
β	:	Relative flow angle [deg]
η	:	Efficiency
ρ	:	Density [kg/m³]
φ	:	Blade setting angle [deg]
ψ	:	Crowding coefficient

Subscripts

1	:	Inlet of blade
2	:	Outlet of blade
3	:	Inlet of guide vane

References

[1] J. Hu, S. Huang and P. S. Wang, Research on hydrodynamic characteristics of axial waterjet pump with guide vane. *Journal of Hydroelectric Engineering*, 2 (2008) 32-36.

[2] F. P. Tang and G. Q. Wang, Influence of Outlet Guide Vanes upon Performances of Water jet Axial-Flow Pump. *Journal of Ship Mechanics*, 6 (2006) 19-26.

[3] L. Belt and T. Cousot, Semi-Spiral Casing and Runner Navier-Stokes Simulation for a Refurbishment Project. *Proc, of the 19th the LAHR Symposium*. Singapore, (1998) 258-267.

[4] F. J. Wang, Y. J. Li and Y. L. Wang, CFD Simulation of 3D flow in large-bore axial-flow pump with half-elbow suction sump. *Journal of Hydrodynamics*, 18 (2) (2006) 243-247.

[5] Blanco M. Numerical flow simulation in a centrifugal pump with impeller-volute interaction. *ASME 2000 Fluid Engineering Division Summer Meeting*, Boston, Massachusetts, June, (2000) 11-15.

[6] S. N. Shukla and J. T. Kshirsagar. Numerial experiments on

a centrifugal pump.*ASME Fluids Engineering Division (Publication) FED*, 257 (2B) (2002) 709-720.

[7] H. X. Chen. Research on turbulent flow within the vortex pumps. *Journal of Hydrodynamic: Ser B*, 16 (6) (2004) 701-707.

[8] B. E. Launder and D. B. Spalding. The Numerical Computation of Turbulent Flows. *Computer Methods in Applied Mechanics and Engineering*, 3 (1974) 269-289.

[9] Z. Wang and W. M. Liu, Two Modificatory K-ε Turbulence Models for Turbulent Swirling Flows. *Journal of Hydrodynamics*, 2 (2003) 51-57.

[10] Y. Victor and O. Steven, A. Renormalization group analysis of turbulence : basic theory.*Journal of Scientific Computing*, 1 (1) (1986) 3-11.

[11] S. V. Patanker, *Numerical heat transfer and fluid flow.* Hemiphere, Washington, (1980) 131-134.

[12] S. V. Patanker and D. B. Spalding, A calculation procedure for heat, mass and momentum transfer in three-dimensional parabolic flows.*Int J Heat Mass Transfer*, 15 (1972) 1787-1806.

[13] M. Ishida, D. Sakaguchi and Z. Sun. Suppression of rotating stall in vaneless diffuser by wall roughness control. *Proceedings of the international Conference on Pumps and Fans.ICPE*, (1998) 232-241.

[14] M. Yaras, Y. K. Zhu and S. A. Sjolander, Flow field in the tip gap of a planar cascade of turbine blades.*ASME Journal of Turbomachinery*, 111 (3) (1989) 276-283.

[15] X. F. Guan, *Modern pump technical manual.* Beijing: China Astronautics Publishing House, (1995) 332-335.

Zhong-Dong Qian is a Professor at the School of Water Resources and Hydropower Engineering at Wuhan University, China. He received his Ph.D. degree in Thermal Engineering from Northern Eastern University in 2002. He has research experience from 2002 to 2004 at Tsinghua University as a postdoctoral researcher. His teaching and research areas include computational fluid dynamics, hydraulic machinery and hydrodynamics.

Young-Ho Lee received his B.E. and M.E. degrees from Korea Maritime University, Korea. He received his Ph.D. in Engineering from the University of Tokyo, Japan. Dr. Lee is currently a Professor at the Division of Mechanical and Information Engineering, Korea Maritime University. His research interests include ocean energy, wind energy, small hydro power, fluid machinery, PIV, and CFD.